Journal of Materials Chemistry

Cite this: *J. Mater. Chem.*, 2012, **22**, 2188

www.rsc.org/materials

**PAPER**

# Solventless thermal decomposition of ferrocene as a new approach for one-step synthesis of magnetite nanocubes and nanospheres

**Daniel Amara, Judith Grinblat and Shlomo Margel***

***Received 13th August 2011, Accepted 31st October 2011***
**DOI: 10.1039/c1jm13942h**



Magnetite ($Fe_3O_4$) nanocubes and nanospheres were synthesized by solventless thermal decomposition of various mixtures of ferrocene and polyvinylpyrrolidone (PVP). Magnetite nanocubes were prepared by grinding and mixing solid mixtures of ferrocene and PVP. The mixtures were then annealed at 350 °C for 2 h in a sealed cell. The nanocubes' size was controlled by adjusting the [ferrocene]/[PVP] weight ratio. Increasing the annealing time to 4 h when the [ferrocene]/[PVP] weight ratio was 1 : 5 led to the formation of magnetite nanospheres. The formed nanocubes/spheres exhibit ferromagnetic behavior at room temperature. The magnetite nanocubes/spheres were formed by a CVD reaction through which the ferrocene molecules, which are in the gas phase at the reaction conditions, decomposed to magnetite nanocubes/spheres dispersed in the solid PVP matrix. The described method offers a new simple, single-step process for the preparation of magnetite nanocubes/spheres. This approach will be extended in future work for one-step synthesis of other metal oxide nanocubes/spheres, *e.g.*, ZnO, $Bi_2O_3$, *etc.*

## Introduction

Magnetic nanoparticles have been intensively studied in recent years due to their unique chemical and physical properties, which differ significantly from those of the bulk materials. This led to a broad range of applications such as hyperthermia,[1,2] information storage media,[3,4] magnetic resonance imaging (MRI),[5] biomedical applications,[6] and catalysis.[7] The shape, size and size distribution of the magnetic materials are the key factors that determine their chemical and physical properties. Thus, the development of size- and shape-controlled magnetic materials became very important for end use. Iron and its oxides are the most useful among the ferromagnetic and the ferrimagnetic elements; Fe has the highest magnetic moment at room temperature, and a Curie temperature that is sufficiently high for the vast majority of practical applications. In addition, iron is a widespread element, and therefore significantly cheaper than other ferromagnetic elements such as nickel and cobalt.[8] Iron oxides such as magnetite ($Fe_3O_4$) and maghemite ($\gamma$-$Fe_2O_3$) are considered as being biocompatible and non-toxic, and therefore possess a broad range of potential biomedical applications.[9–11] Magnetic nanoparticles tend to aggregate due to a strong magnetic dipole–dipole and van der Waals attraction. Thus, the main challenge in the synthesis process is to overcome these aggregation phenomena. This is usually done by coating the nanoparticle's surface with the desired functional polymers or surfactants. The surfactant also plays a role in the nucleation process and in limiting particle growth. The functional groups belonging to the organic coating also allow the binding of biological molecules, such as proteins, oligonucleotides, *etc.*, to the particle's surface for biomedical applications.[12] Iron and iron-oxide nanoparticles are typically prepared by the decomposition of soluble iron precursors in solutions containing an appropriate stabilizer. The decomposition of the iron precursors is accomplished by means of processes such as sonochemistry,[7,13,14] thermal decomposition,[15] electrochemical[16] and laser decomposition.[17] Among the iron precursors, iron carbonyl compounds are the most useful ones, since they can easily decompose and release CO molecules, which can easily be removed from the reaction mixture. Recently, we published a novel method for the preparation of superparamagnetic and ferromagnetic iron oxide and Fe nanoparticles by the thermal decomposition of triiron dodecacarbonyl in diethylene glycol diethyl ether with oleic acid as a stabilizer.[18,19] Han *et al.* recently published a novel method to synthesize highly magnetized iron nanoparticles by a solventless thermal decomposition method of iron oleate at 400 °C.[20] The formed iron oxide nanoparticles were then solventless reduced into $\alpha$-Fe nanoparticles by hydrogen in the presence of sodium chloride as a separating medium. Ferrocene, $Fe(C_5H_5)_2$, is an organometallic sandwich compound consisting of two cyclopentadienyl rings bound to opposite sides of an iron atom. It is an air-stable orange solid that readily sublimes.[21] Recently, we published a novel method for the synthesis of porous superparamagnetic and ferromagnetic iron oxide composite nano/microspheres of narrow size distribution, by solventless thermal decomposition of ferrocene.[22] The nano/microparticles were prepared by entrapping *via* vacuum separating media and then

*Institute of Nanotechnology & Advanced Materials, Department of Chemistry, Bar-Ilan University, 52900 Ramat Gan, Israel. E-mail: shlomo.margel@mail.biu.ac.il; amara.daniel@gmail.com; Fax: +972-3-7384053; Tel: +972-3-5318994*

ferrocene within porous poly(divinyl benzene) microspheres, followed by thermal decomposition of the entrapped ferrocene and then removing the separating media. The present manuscript describes a novel simple one-step method to prepare magnetite nanocubes and nanospheres. This was accomplished by solventless thermal decomposition under different conditions of ferrocene in the presence of PVP. Characterization of the formed nanocubes/spheres was accomplished by routine methods such as TEM, elemental analysis, XRD, SQUID, TGA, and DSC.

## Experimental section

### Materials

Ferrocene (>98%), polyvinylpyrrolidone (PVP, $M_w$ 360 000) and ethanol (HPLC) were purchased from Aldrich (Israel) and were used without further purification.

### Synthesis of magnetic nanocubes and nanospheres

$Fe_3O_4$ nanocubes were formed by grinding mixtures of ferrocene and PVP of various weight ratios (1 : 1, 1 : 2 and 1 : 5). 300 mg of the solid mixtures were then introduced into a 1 ml stainless steel sealed cell. The solid mixtures were then introduced into a tube furnace preheated to 350 °C for 2 h in ambient atmosphere. The sealed cell was then cooled to room temperature and the resulting black powder was collected. The obtained magnetite nanocubes were then washed from excess reagents by extensive centrifugation cycles with ethanol. $Fe_3O_4$ nanospheres were obtained by a similar solventless process by increasing the annealing time to 4 h at a [PVP]/[ferrocene] weight ratio of 5 : 1.

### Characterization of the magnetic nanocubes and nanospheres

Transmission Electron Microscope (TEM) images were obtained by employing a 200 kV JEOL-2100 device. The average size and size distribution of the magnetite nanocubes and nanospheres of the electronic images were determined by measuring the diagonal length or diameter, respectively, of more than 100 cubes per spheres with Image Analysis software, AnalySIS Auto (Soft Imaging System GmbH, Germany). C, H and O analysis of the various nanocubes/spheres was performed using an elemental analysis instrument, model FlashEA1112 Instruments, Thermoquast. Powder X-ray diffraction (XRD) patterns were recorded using an X-ray diffractometer (model D8 Advance, Bruker AXS) with Cu K$\alpha$ radiation. Isothermal magnetization measurements at room temperature were performed in a commercial (Quantum Design) super-conducting quantum interference device (SQUID) magnetometer. Mössbauer studies were performed using a conventional constant acceleration drive and a 50 mCi $^{57}$Co:Rh source. The velocity calibration was performed using a room temperature $\alpha$-Fe absorber, and the isomer shift (I.S.) values are relative to that of iron. The observed spectra were least-square fitted by theoretical spectra, assuming a distribution of hyperfine interaction parameters, corresponding to non-equivalent iron locations differing in local environment. Fourier transform infrared (FTIR) analysis was performed with a Bruker FT-IR Spectrometer model ALPHA-P. The analysis was performed with 13 mm KBr pellets that contained 2 mg of the detected material and 198 mg of KBr. The thermal behavior of the PVP was measured by Thermo Gravimetric Analysis (TGA) and Differential Scanning Calorimetry (DSC), STAR-1 System, Mettler Toledo. The thermal analysis was preformed under ambient atmosphere at a heating rate of 5 °C min$^{-1}$.

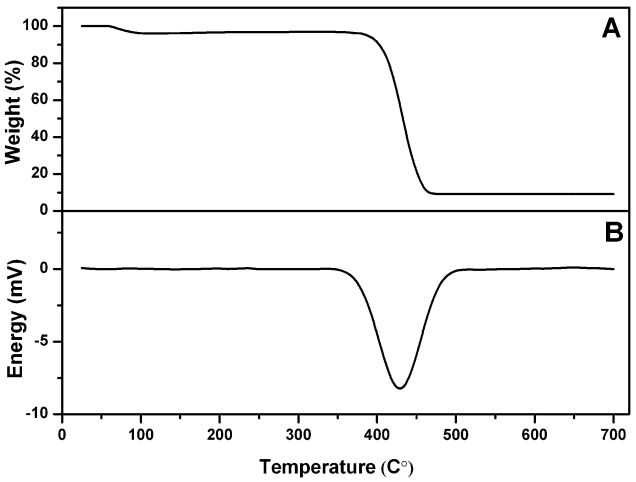


**Fig. 1** TGA (A) and DSC (B) thermograms of the PVP.

## Results and discussion

Magnetic nanocubes/spheres were formed by solventless thermal decomposition of ferrocene at 350 °C within a sealed cell in the presence of PVP. The PVP was used as a separating medium and stabilizer of the formed iron-oxide nanocubes/spheres. Fig. 1A and B show the thermal behaviour of the PVP. The TGA curve (A) exhibits a steep slope between 400 and 450 °C, indicating a 91% weight loss due to PVP decomposition, leaving residual

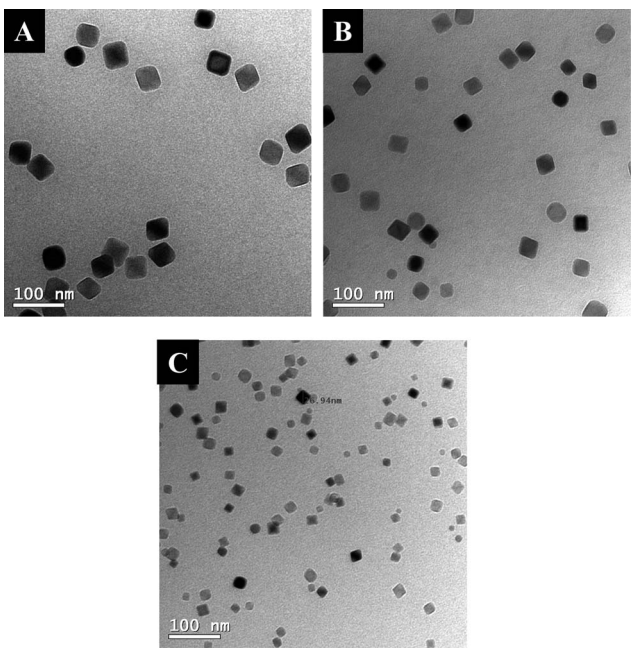


**Fig. 2** TEM micrographs of the iron oxide nanocubes obtained by thermal decomposition at 350 °C for 2 h of solid mixtures of ferrocene and PVP of weight ratios of 1 : 1 (A), 1 : 2 (B) and 1 : 5 (C).

**Table 1** Elemental analysis, size and size distribution of the nanocubes/spheres obtained by annealing different ratios of ferrocene and PVP mixtures for different time periods[a]

| | | | Mass% | | | | |
|---|---|---|---|---|---|---|---|
| [Ferrocene]/[PVP] (w/w) | Annealing time (h) | Size (nm) | C | O | N | Fe | $[Fe_3O_4]/[Fe_3O_4 + PVP]$ |
| 1 : 1 | 2 | 49 ± 4.0 | 31.1 | 21.6 | 6.5 | 37 | 51 |
| 1 : 2 | 2 | 41 ± 5.2 | 46.5 | 18.4 | 8.9 | 20.3 | 28 |
| 1 : 5 | 2 | 29 ± 3.4 | 54.2 | 17.4 | 10.6 | 11.5 | — |
| 1 : 5 | 4 | 32 ± 5.4 | 57 | 16.1 | 11 | 8.8 | 12.1 |

[a] The magnetite nanocubes/spheres were prepared according to the Experimental part. The size of the nanocubes and the nanospheres relates to the diagonal length of the cubes and the diameter of the spheres, respectively. The Fe amount was calculated by reducing the sum of the other elements from 100.

carbon. This observation is in good agreement with the DSC curve (B) that exhibits an endothermic peak around 430 °C, related to the decomposition of the polymer. TGA isothermal measurements at 350 °C for 2 h at ambient atmosphere also did not exhibit any significant weight loss of the PVP. These thermogravimateric studies demonstrate the durability of the PVP at the annealing temperature of 350 °C at which the ferrocene decomposed to give magnetic iron oxide nanocubes/spheres. TEM images of nanocubes obtained by thermal decomposition at 350 °C for 2 h of solid mixtures of ferrocene and PVP of weight ratios of 1 : 1, 1 : 2 and 1 : 5 are presented in Fig. 2A–C, respectively. The images demonstrate the cubic morphology of the obtained nano-iron oxides. Moreover, the images clearly demonstrate that the size of the nanocubes depends directly on the [ferrocene]/[PVP] weight ratio. The nanocubes' size, as measured by the diagonal length of the cubes, decreased from 49 ± 4 to 41 ± 5.2 and 29 ± 3.4 nm as the [ferrocene]/[PVP] weight ratio decreased from 1 : 1 to 1 : 2 and 1 : 5, respectively (see Table 1 and Fig. 3). It should be noted that the ferrocene has a boiling point of 249 °C and the various nanocubes were formed at 350 °C. Thus, the decomposition of the ferrocene was accomplished in the gas phase, resulting in the formation of the nanocubes in the PVP domain that is stable at this temperature, as confirmed by thermogravimetric measurements (Fig. 1). This process is actually a chemical vapor deposition (CVD) reaction in which the ferrocene is the volatile precursor and the PVP is the solid substrate. Moreover, the TEM images clearly demonstrate individual nanocubes for the various samples. This may suggest that the solid PVP matrix is used in this process as a separating medium during the decomposition of the ferrocene to form the iron oxide nanocubes. It is remarkable that the decomposition temperature of ferrocene is above 450 °C, and annealing the ferrocene at 350 °C for 2 h in a sealed cell in the absence of PVP did not lead to the decomposition of the organometallic compounds. However, the thermal decomposition of ferrocene in the presence of PVP leads to its decomposition to iron-oxide nanocubes/spheres. This may imply that the PVP catalyzes the thermal decomposition of the ferrocene. Fig. 4A and B show by low and high magnification TEM pictures the perfect spherical shape of the nanospheres of 32 ± 5.4 nm obtained by annealing the solid mixture of ferrocene and PVP of a 1 : 5 weight ratio for 4 h. On the other hand, to our surprise, annealing of the other solid mixtures of the ferrocene and PVP of 1 : 1 and 1 : 2 weight

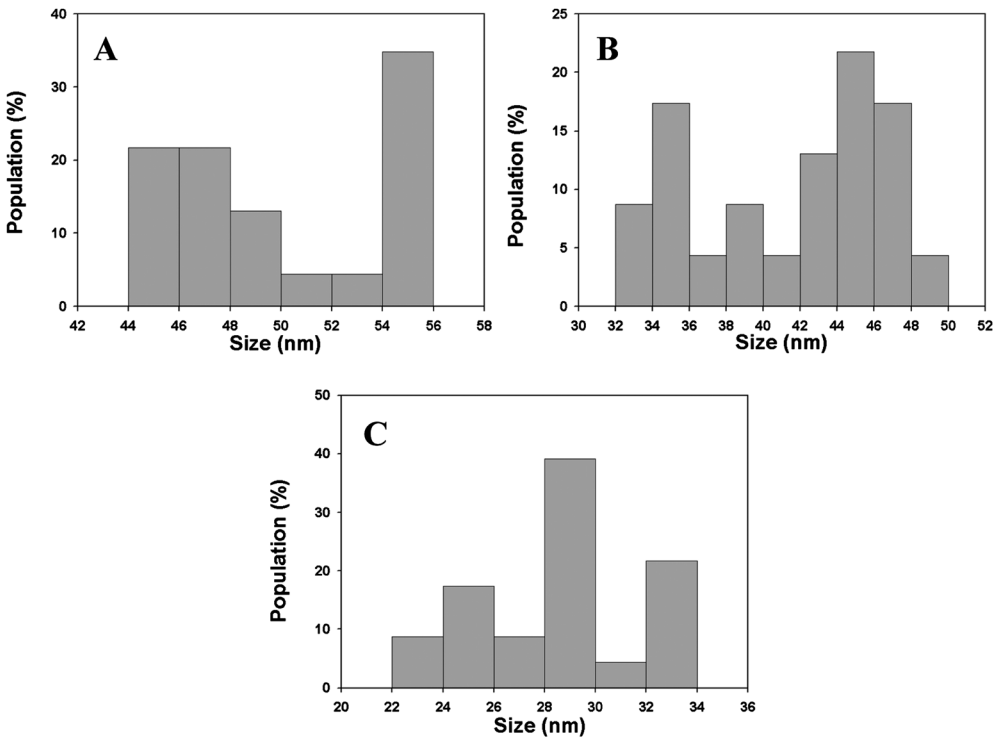


**Fig. 3** Size distribution of the nanocubes obtained by thermal decomposition at 350 °C for 2 h of solid mixtures of ferrocene and PVP of weight ratios of 1 : 1 (A), 1 : 2 (B) and 1 : 5 (C).

 

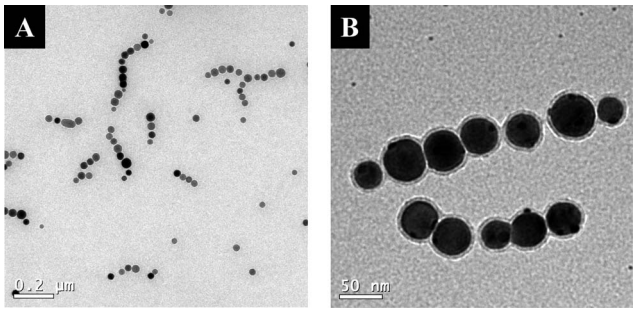


**Fig. 4** Low (A) and high (B) magnification TEM micrographs of the iron oxide nanospheres obtained by thermal decomposition at 350 °C for 4 h of a solid mixture of ferrocene and PVP of a weight ratio of 1 : 5.

ratios for 4 h did not alter their cubic shape to spheres. Fig. 4B demonstrates a core–shell architecture of the iron oxide spherical particles. The core is composed of the iron-oxide phase, while the shell is composed of the PVP. Fig. 5A–D illustrate the XRD patterns of the iron nanocubes/spheres obtained by thermal decomposition at 350 °C for 2 or 4 h of solid mixtures of ferrocene and PVP of weight ratios of 1 : 1 (A), 1 : 2 (B) and 1 : 5 (C and D). The nanocubes (A, B, and C) were formed by the thermal decomposition of the ferrocene for 2 h, and for 4 h for the nanospheres (D). Fig. 5 A, B and D demonstrate well the crystallized iron-oxide phases of the nanocubes/spheres. On the other hand, Fig. 5C demonstrates an iron-oxide phase which is not well crystallized. In addition, this pattern demonstrates the presence of a small impurity fraction of FeO. All the XRD patterns can be attributed either to magnetite ($Fe_3O_4$) or to maghemite ($\gamma$-$Fe_2O_3$), because of the similarity in their XRD patterns. Thus, Mössbauer spectroscopy (MS) at RT was employed and showed that this fraction was indeed composed of the $Fe_3O_4$ phase, as described below. Thus, all the XRD patterns were indexed as magnetite. Table 1 demonstrates the mass% of C, H, O, N and Fe, as well as the size and size distribution of the

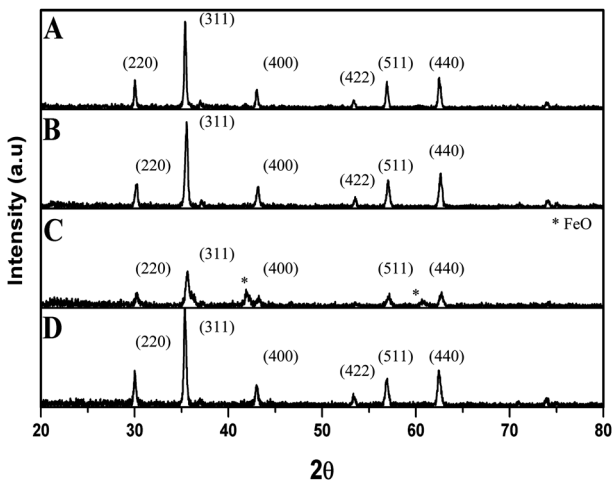


**Fig. 5** XRD patterns of the magnetite nanocubes/spheres obtained by thermal decomposition at 350 °C for 2 or 4 h of solid mixtures of ferrocene and PVP of weight ratios of 1 : 1 (A), 1 : 2 (B) and 1 : 5 (C and D). The nanocubes (A, B and C) were formed by thermal decomposition of the ferrocene for 2 h, and the nanospheres (D) for 4 h, according to the Experimental part.

different nanocubes/spheres. A simple calculation indicates that the weight ratio of [Fe]/[O] in magnetite is 2.62/1. Thus, the % magnetite content of the nanocubes obtained by the thermal decomposition at 350 °C for 2 h of solid mixtures of ferrocene and PVP of weight ratios of 1 : 1 and 1 : 2 and of the nanospheres obtained by thermal decomposition at 350 °C for 4 h of a solid mixture of ferrocene and PVP of a weight ratio of 1 : 5 are 51, 28 and 12.1%, respectively. Table 1 also exhibits that the [C] : [H] : [N] : [O] (oxygen belonging to the PVP only) weight ratios of these nanocubes/spheres are 8.2 : 1.0 : 1.7 : 2.0, 7.9 : 1.0 : 1.5 : 1.8 and 8.0 : 1.0 : 1.5 : 1.8, respectively. These ratios are almost the same as those calculated for pure PVP ($C_6H_9NO$). The % magnetite content of the nanocubes obtained by the thermal decomposition for 2 h of solid mixtures of ferrocene and PVP of a weight ratio of 1 : 5 cannot be calculated due to the presence of small FeO phase impurity as shown previously by the XRD measurements. It should be noted that the mixtures obtained after decomposition of the various ferrocene/PVP mixtures, before ethanol washing, did not indicate the presence of ferrocene traces, as verified by FTIR spectra (by the absence of the ferrocene peaks for example at 3922, 2253, 1776 $cm^{-1}$, *etc.*). The yield of the ferrocene decomposition to iron oxide was almost 100% whereas excess PVP was removed by ethanol washing. Thus, the [PVP] : [Fe] weight ratios are lower than their original ratios in the reagents as shown in Table 1. Fig. 6A–D exhibit the RT MS spectra of the nanocubes/spheres obtained by thermal decomposition at 350 °C for 2 and 4 h of solid mixtures of ferrocene and PVP of weight ratios of 1 : 1, 1 : 2, and 1 : 5, and for the nanospheres obtained by thermal decomposition at 350 °C for 4 h of a solid mixture of ferrocene and PVP of a weight ratio of 1 : 5, respectively. All the samples exhibit two magnetic sextets with I.S. = 0.29 and 0.69 mm $s^{-1}$ and $H_{eff} = 490 \pm 5$ and $460 \pm 5$ kOe, respectively, which are related to the two crystallographic sites of magnetite. However, the particles obtained by thermal decomposition at 350 °C for 2 h of ferrocene and PVP with a weight ratio of 1 : 5 for 2 h contain 31% of small particles above the blocking temperature. The effect of the PVP concentration and reaction time on the particles size can be explained as follows: previous studies have demonstrated by FT-IR spectrometry that PVP molecules may coordinate with metal ions to form a stable metal–PVP complex.[23,24] The PVP used in this study probably influences the nucleation, growth and aggregation of the obtained magnetite crystallites, by forming iron–PVP complex molecules. This complex formation may explain the effect of PVP concentration on the size and morphology of the formed magnetite nanocubes/spheres. The generation of this complex inevitably increases the time for iron atoms to reach supersaturation and to their final size. This means that the growth rate of the magnetite crystallites will decrease as their faces adsorbed PVP molecules, because the crystal growth rate is generally lowered with adsorbed polymer.[25] Moreover, the number of 'free sites' on the PVP surface that can serve as binding sites to form the iron–PVP complex increases with increasing the PVP concentration, thereby resulting in nanocubes/spheres of decreasing size. The PVP concentration and the annealing time are also probably the key factors in explaining the shape alteration of the magnetite crystallites, by effecting crystal growth in different directions. It is known that the crystal growth rate generally decreases with the adsorbed polymer, and crystallite morphology can be altered by the presence of polymer specifically

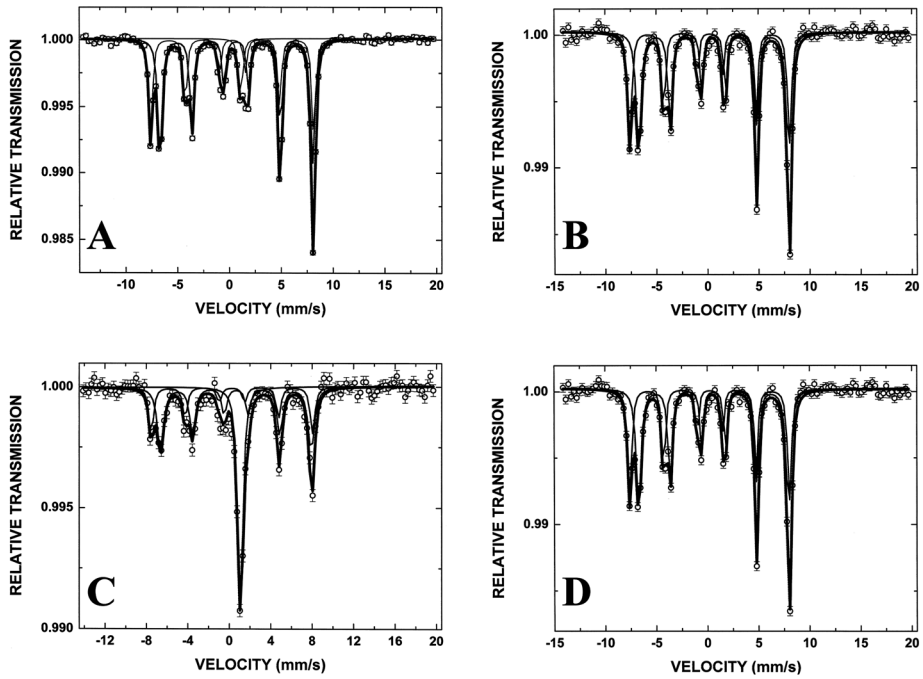


**Fig. 6** Mössbauer spectra at room temperature of the magnetite nanocubes/spheres obtained by thermal decomposition at 350 °C for 2 or 4 h of solid mixtures of ferrocene and PVP of weight ratios of 1 : 1 (A), 1 : 2 (B) and 1 : 5 (C and D). The nanocubes (A, B and C) were formed by thermal decomposition of the ferrocene for 2 h and 4 h for the nanospheres (D), according to the Experimental part.

interacting with the crystal faces.[26] Magnetite was formed as cubes when the growth in some direction was restricted by the adsorbed PVP molecules, while one direction was free to allow growth. This led to the formation of nanocubes. In contrast, magnetite nanospheres were formed when the annealing time increased, allowing the growth of the crystallites in different directions. Previous studies reported that a shift of carbonylband was observed in the IR spectra of PVP in the presence of various metal ions. According to these previous studies this band shift is due to the interaction between the carbonyl oxygen of PVP and the metal ions.[27–29] Indeed, a pure PVP spectrum demonstrates a C═O band at 1650 $cm^{-1}$ (Fig. 7A) while the various nanocubes/spheres demonstrated this carbonyl peak at 1644 $cm^{-1}$, a shift of 6 $cm^{-1}$ (Fig. 7B). Please note that Fig. 7B illustrates the carbonyl PVP peak of the magnetite nanocubes obtained by thermal decomposition at 350 °C for 2 h of a solid mixture of ferrocene and PVP of a weight ratio of 1 : 5. However, the same carbonyl peak was also observed for the other nanocubes/spheres.

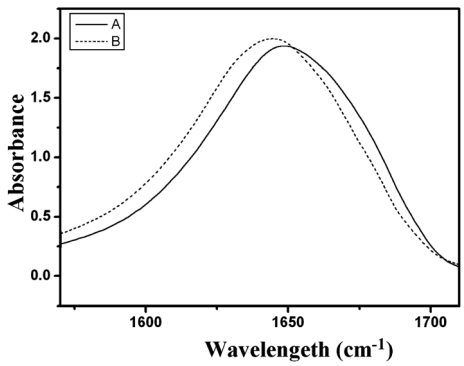


**Fig. 7** FT-IR spectra of the carbonyl peaks of pure PVP(A) and of the magnetite nanocubes obtained by thermal decomposition at 350 °C for 2 h of a solid mixture of ferrocene and PVP of a weight ratio of 1 : 5.

The carbonyl peak shift in the nanocube/sphere samples probably implies the formation of the Fe-PVP complex which directly relates to the previously suggested mechanism. Fig. 8 represents the isothermal field dependent on or independent of the magnetization measured at 300 K. The hysteresis loops for the magnetite nanocubes/spheres are presented in curves A–D.

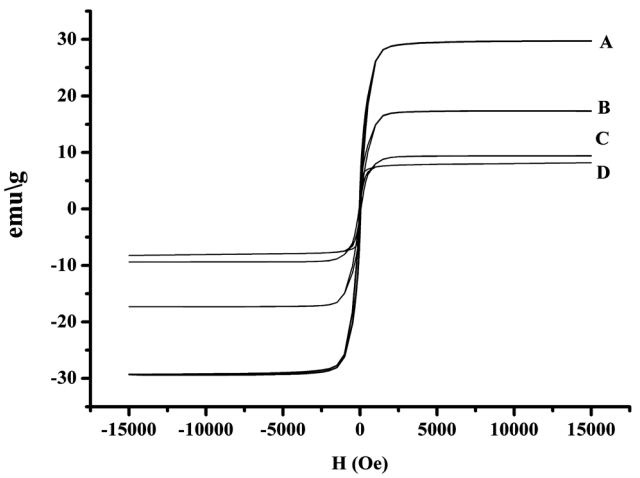


**Fig. 8** Magnetization (*M*) *vs.* magnetic field (*H*) at 300 K of the magnetite nanocubes/spheres obtained by thermal decomposition at 350 °C for 2 or 4 h of solid mixtures of ferrocene and PVP of weight ratios of 1 : 1 (A), 1 : 2 (B) and 1 : 5 (C and D). The nanocubes (A, B and C) were formed by thermal decomposition of the ferrocene for 2 h, and 4 h for the nanospheres (D), according to the Experimental part.

 

**Table 2** Magnetic properties of the nanocubes/spheres obtained by annealing different ratios of ferrocene and PVP mixtures for different time periods[a]

| [Ferrocene]/ [PVP] (w/w) | Annealing time (h) | $M_s$ (emu $g^{-1}$) | Coercivity (Oe) |
|---|---|---|---|
| 1 : 1 | 2 | 29.7 | 50 |
| 1 : 2 | 2 | 17.3 | 40 |
| 1 : 5 | 2 | 9.4 | 36 |
| 1 : 5 | 4 | 8.2 | 15 |

[a] The magnetite nanocubes/spheres were prepared according to the Experimental part. The size of the nanocubes and the nanospheres relates to the diagonal length of the cubes and the diameter of the spheres, respectively.

The magnetic saturation moments ($M_s$), as well as the coercive fields of these particles, are shown in Fig. 8 and summarized in Table 2. The $M_s$ values obtained at 300 K are 29.7, 17.3 and 9.4 emu $g^{-1}$, for the magnetite nanocubes obtained by the thermal decomposition of mixtures of ferrocene and PVP of 1 : 1, 1 : 2 and 1 : 5 weight ratios, respectively, and 8.2 emu $g^{-1}$ for the magnetite nanospheres. By subtracting the PVP content, the calculated $M_s$ values in terms of emu per g of $Fe_3O_4$ are 58.2 and 61.7 for the nanocubes obtained by the thermal decomposition of mixtures of ferrocene and PVP of 1 : 1 and 1 : 2, respectively, and 67.8 for the nanospheres (the value for the nanocubes obtained by the thermal decomposition for 2 h of a solid mixture of ferrocene and PVP of a weight ratio of 1 : 5 cannot be calculated due to the presence of FeO impurity). It should be noted that the $M_s$ bulk value of magnetite is 92 emu $g^{-1}$.[30] The relatively lower $M_s$ values of the magnetic nanocubes/spheres compared to the bulk values arise from the non-magnetic PVP content, which leads to the decrease in the magnetization per weight. Another explanation for the relatively low magnetization values is the surface effect that can occur in the case of magnetic core and non-magnetic shell structures. This effect leads to the reduction in the magnetic moment by a different mechanism, *e.g.*, the existence of a magnetically dead layer on the cubes/spheres' surface, the existence of canted spins, or the existence of a spin glass-like behavior of the surface spins.[31] The merging temperature of the two ZFC/FC branches is defined as the blocking temperature ($T_b$) of superparamagnetic particles. Fig. 9 shows the FC and ZFC curves of the nanocubes obtained by thermal decomposition at 350 °C for 2 h of a solid mixture of ferrocene and PVP of a weight ratio of 1 : 5. The two curves tend to merge around 210 K (which is taken as $T_b$), but no complete overlap is observed up to 300 K, indicating the existence of both superparamagnetic and ferromagnetic phases in this material. This observation is in a good agreement with the Mössbauer studies.

The structure of the obtained nanocubes/spheres was also investigated in HRTEM mode using either the conventional selected area electron diffraction (SAED) and nano-beam (NBD) diffraction technique or Fourier Transform Analysis (FFT) of high resolution images, depending on the size and the orientation of the materials. The two possible oxides maghemite ($\gamma$-$Fe_2O_3$) and magnetite ($Fe_3O_4$) are structurally similar; hence they cannot be distinguished according to their electron diffraction patterns. All our electron diffraction patterns could be indexed in terms of the FCC structure of both maghemite and magnetite, $a = 8.34$ Å

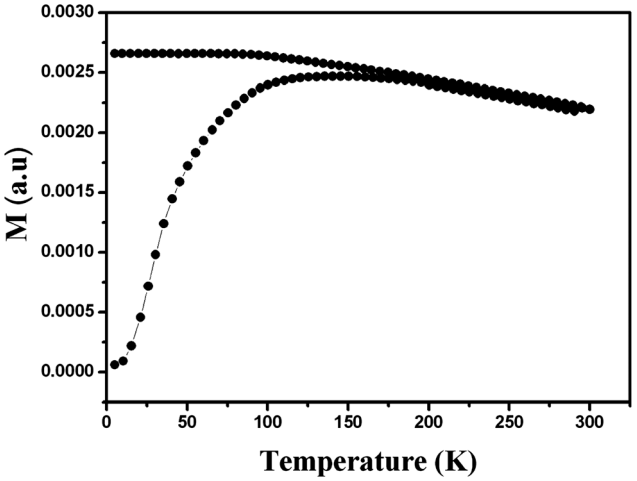


**Fig. 9** Zero field cooled (ZFC) and field (FC) cooled temperature dependent magnetization of the nanocubes obtained by thermal decomposition at 350 °C for 2 h of solid mixtures of ferrocene and PVP of a weight ratio of 1 : 5.

and $a = 8.39$ Å (PDF#000391346 and PDF#010890950), respectively. The Mössbauer spectra results provided the supporting evidence that the resulting compounds are indeed magnetite. Fig. 10A is a high resolution electron micrograph (HRTEM) of a typical single crystalline nanocube obtained by thermal decomposition of a 1 : 1 weight ratio of a ferrocene and PVP mixture. This figure displays lattice-fringe contrast of the $d_{022}$ family of planes (0.3 nm). The nanocube was identified and characterized using the SAED pattern shown in Fig. 10B. This electron diffraction pattern was taken from an area of 300 nm comprising several nanocubes and it shows a typical ring diffraction pattern as expected from polycrystalline materials. The marked reflections correspond to the interplanar spacings, $d_{220}$, $d_{311}$ and $d_{400}$ in the FCC structure of magnetite $Fe_3O_4$ $a = 8.39$ Å and the pattern was indexed as magnetite. Fig. 10C and E are the HRTEM micrographs of individual $Fe_3O_4$ nanocubes obtained by thermal decomposition of 1 : 2 and 1 : 5 weight ratios of ferrocene and PVP mixtures for 2 h, respectively. Both nanocubes display well resolved lattice-fringe contrast as displayed in the respective figures (Fig. 10C and D) and their identification was based on the analysis of these high resolution images. The inset on the top right in Fig. 10C is the computed Fourier transform of the portion of the image outlined by the white square which, like a diffraction pattern, was indexed on the basis of the unit cell of magnetite. Marked are the $d_{022}$ and $d_{113}$ family of planes. The inset on the bottom right represents the filtered and magnified portion of the image outlined by the square. The distances measured between lattice fringes were 0.3 nm ($d_{022}$) and 0.25 nm ($d_{113}$) of the cubic FCC structure of $Fe_3O_4$ ($a = 8.35$ Å). Fig. 10E shows the lattice fringe $d_{113}$ (0.25 nm) plane of the nanocubes obtained by 1 : 5 weight ratios of ferrocene and PVP for 2 h. Fig. 10D and F are the NBD patterns taken from the nanocubes obtained by thermal decomposition of 1 : 2 and 1 : 5 weight ratios of ferrocene and PVP for 2 h, respectively. All NBD patterns were taken from a nano-area of 4–7 nm of the nanocubes. The NBD pattern (10D) shows sets of reflections for $d_{022}$ planes and $\langle d_{113} \rangle$ family of planes and the

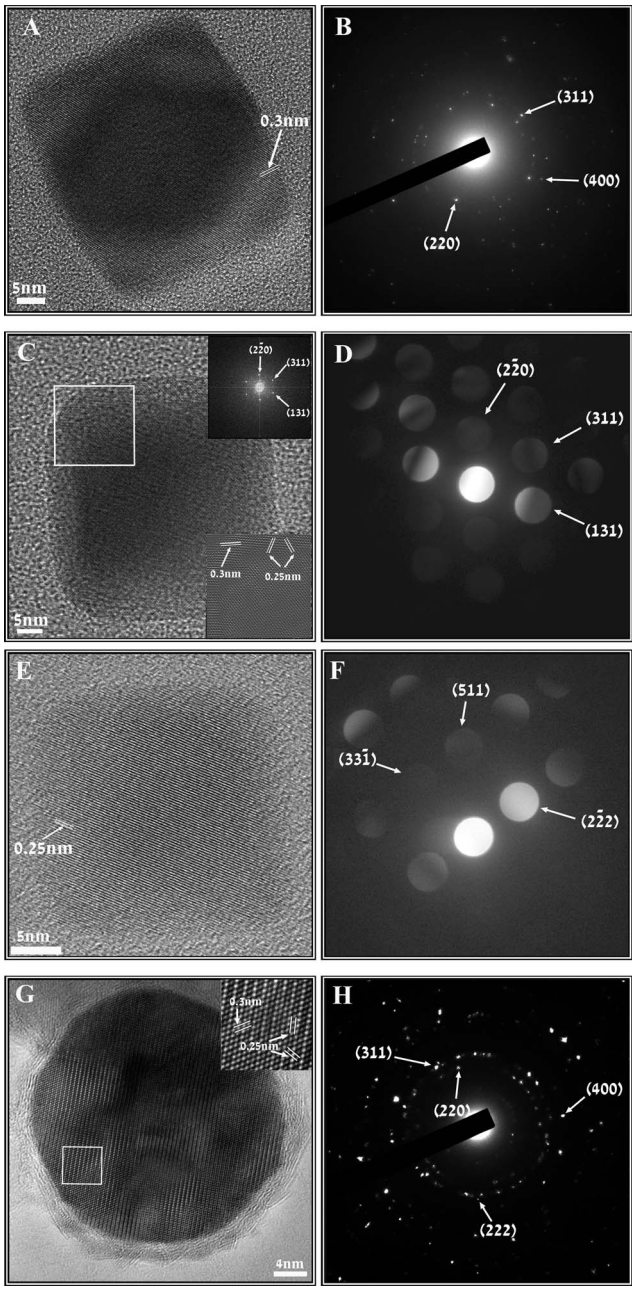


**Fig. 10** High resolution electron micrograph of typical magnetite nanocubes/spheres obtained by thermal decomposition at 350 °C for 2 or 4 h of solid mixtures of ferrocene and PVP of weight ratios of 1 : 1 (A), 1 : 2 (C) and 1 : 5 (E and G) and the corresponding ED pattern (B, D, F and H, respectively). The nanocubes (A–F) were formed by thermal decomposition of ferrocene for 2 h, and 4 h for nanospheres (G and H), according to the Experimental part. The inset marked by the white square (C and G) is the magnified image and Fourier transform taken from the area (C).

NBD pattern (10F) shows sets of reflections for $d_{222}$, $d_{133}$ and $d_{115}$ planes. These patterns were also indexed according to the FCC cubic structure of $Fe_3O_4$. Fig. 10G is the HRTEM micrograph of a crystalline $Fe_3O_4$ nanosphere coated with a thin amorphous layer of PVP. The inset represents the magnified portion of the image outlined by the white square. The distances measured between lattice fringes were 0.24 nm and 0.25 nm matching the interplanar spacings for $d_{222}$ and $d_{113}$ family of planes, respectively. Fig. 10H is the SAED pattern taken from several nanospheres showing reflections that correspond to the interplanar spacing, $d_{220}$, $d_{311}$, $d_{222}$ and $d_{400}$, and was indexed on the basis of the FCC structure of magnetite. Utilization of these advanced nano-techniques, together with the Mössbauer spectra results, provided unambiguous evidence that the resulting compounds are the FCC structure magnetite with unit cell parameter $a = 8.39$ Å.

## Summary and conclusions

This manuscript describes a novel, simple process for the preparation of monodisperse magnetite nanocubes and nanospheres, by a single-step solventless thermal decomposition of ferrocene in the presence of PVP. This work demonstrates that the shape and size of the formed magnetite can be controlled by adjusting the [PVP]/[ferrocene] weight ratio and the ferrocene decomposition reaction time period. This manuscript presents preliminary studies. Further extension of this work is ongoing in our laboratory, in order to better understand the reason for obtaining cubes and the change to a spherical shape. We also plan on extending this work for the one-step synthesis of other metal oxide nanocubes/spheres, *e.g.*, ZnO, $Bi_2O_3$, *etc.*

## Acknowledgements

This study was partially supported by a Minerva Grant (Microscale & Nanoscale Particles). Thanks to Prof. Israel Felner from The Racah Institute of Physics, Hebrew University, Jerusalem, Israel, for his help in the Mössbauer spectroscopy measurements.

## References

1 R. Hergt, R. Hiergeist, I. Hilger, W. A. Kaiser, Y. Lapatnikov, S. Margel and U. Richter, *J. Magn. Magn. Mater.*, 2004, **270**, 345–357.
2 J. P. Fortin, C. Wilhelm, J. Servais, C. Menager, J. C. Bacri and F. Gazeau, *J. Am. Chem. Soc.*, 2007, **129**, 2628–2635.
3 S. Sun, C. B. Murray, D. Weller, L. Folks and A. Moser, *Science*, 2000, **287**, 1989–1992.
4 S. Sun and H. Zeng, *J. Am. Chem. Soc.*, 2002, **124**, 8204–8205.
5 M. C. Bautista, O. Bomati-Miguel, X. Zhao, M. P. Morales, T. Gonzalez-Carreno, R. P. Alejo, J. Ruiz-Cabello and S. Veintemillas-Verdaguer, *Nanotechnology*, 2004, **15**, 154–159.
6 E. Carpenter, *J. Magn. Magn. Mater.*, 2001, **225**, 17–20.
7 S. Suslick, T. Hyeon and M. Fang, *Chem. Mater.*, 1996, **8**, 2172–2179.
8 L. H. Dale, *Small*, 2005, **1**, 482–501.
9 A. Z. Wang, V. Bagalkot, C. Vasilliou, F. Gu, F. Alexis, L. Zhang, M. Shaikh, K. Yuet, M. Cima, R. Langer, P. W. Kantoff, N. H. Bander, S. Jon and O. C. Farokhzad, *ChemMedChem*, 2008, **3**, 1311–1315.
10 C. Stefaniu, M. Chanana, D. Wang, D. V. Novikov, G. Brezesinski and H. Möhwald, *ChemPhysChem*, 2010, **11**, 3585–3588.
11 M. Furlan, J. Kluge, M. Mazzotti and M. Lattuada, *J. Supercrit. Fluids*, 2010, **54**, 348–356.
12 M. V. Yigit, D. Mazumdar and Y. Lu, *Bioconjugate Chem.*, 2008, **19**, 412–417.
13 K. V. Shafi, A. Ulman, X. Yan, N. L. Yang, C. Estournes, H. White and M. Rafailovich, *Langmuir*, 2001, **17**, 5093–5097.
14 S. Wizel, S. Margel and A. Gedanken, *Polym. Int.*, 2000, **49**, 445–448.
15 J. Lai, K. V. Shafi, A. Ulman, K. Loos, Y. Lee, T. Vogt, W. L. Lee and N. P. Ong, *J. Phys. Chem. B*, 2005, **109**, 15–18.
16 D. E. Weisshaar and T. Kuwana, *J. Electroanal. Chem.*, 1984, **163**, 395–399.

 

17 E. Ye, B. Liu and W. Y. Fan, *Chem. Mater.*, 2007, **19**, 3845–3849.
18 D. Amara, I. Felner, I. Nowik and S. Margel, *Colloids Surf., A*, 2009, **339**, 106–110.
19 W. Yu, J. C. Falkner, C. T. Yavuz and V. L. Colvin, *Chem. Commun.*, 2004, 2306–2307.
20 Y. C. Han, H. G. Cha, C. W. Kim, Y. H. Kim and Y. S. Kang, *J. Phys. Chem. C*, 2007, **111**, 6275–6280.
21 A. Federman Neto, A. C. Pelegrino and V. A. Darin, Ferrocene: 50 years of transition metal organometallic chemistry—from organic and inorganic to supramolecular chemistry, *ChemInform*, 2004, **35**, DOI: 10.1002/chin.200443242.
22 D. Amara and S. J. Margel, *J. Mater. Chem.*, 2011, **21**, 15764–15772.
23 Z. T. Zhang, B. Zhao and L. M. Hu, *J. Solid State Chem.*, 1996, **121**, 105–110.
24 B. L. Rivas, E. D. Pereira and I. M. Villoslada, *Prog. Polym. Sci.*, 2003, **28**, 173–208.
25 P. J. Van der Put, in *The Inorganic Chemistry of Materials: How to Make Things Out of Elements*, Plenum, New York, 1998, p. 278.
26 Y. G. Sun and Y. N. Xia, *Science*, 2002, **298**, 2176–2179.
27 J. L. Wuepper and A. L. Popov, *J. Am. Chem. Soc.*, 1969, **91**, 4352–4356.
28 N. H. Agnew, *J. Polym. Sci., Polym. Chem. Ed.*, 1976, **14**, 2819–2830.
29 B. P. Grady, E. M. O'connell, C. Z. Yang and S. L. Cooper, *J. Polym. Sci., Part B: Polym. Phys.*, 1994, **32**, 2357–2366.
30 B. D. Cullity, *Introduction to Magnetic Materials*, Addison-Wesley Pub. Co, Reading, Mass, 1972, p. 200.
31 R. H. Kodama, *J. Magn. Magn. Mater.*, 1999, **200**, 359–372.